Nuclear liquid-gas phase transition in generalized thermo-statistics

K. Miyazaki

E-mail: miyazakiro@rio.odn.ne.jp

Abstract

A new calculus of nuclear liquid-gas phase transition in the standard thermo-statistics is applied to the generalized thermo-statistics. Because the phase equilibrium is defined in terms of intensive temperature and conjugate extensive entropy, we have to solve higher-order simultaneous nonlinear equations than those in the standard thermo-statistics. The features of phase transition are essentially the same as those in the standard thermo-statistics. The phase transition is the first order. There is no critical point in the section of binodal surface. The caloric curve reproduces the experimental data well. We however cannot find the retrograde condensation predicted in the standard thermo-statistics.

The generalized thermo-statistics [1,2] is expected to be applicable to non-equilibrium systems and small systems. Because they are also produced in the multifragmentation reaction [3,4] of heavy ions, the generalized thermo-statistics recently attracts considerable attention [5-11] in nuclear physics. On the other hand, it is well known that [12,13] the asymmetric nuclear matter produced in heavy-ion reaction exhibits liquid-gas phase transition. It is therefore valuable to investigate nuclear liquid-gas phase transition in the generalized thermo-statistics. The asymmetric nuclear matter is a binary system that has two independent chemical potentials of proton and neutron. According to the Gibbs condition on phase equilibrium, both the chemical potentials in liquid and gaseous phases are equilibrated. Within the standard thermo-statistics, the geometrical construction [14-19] is usually used to investigate nuclear liquid-gas mixed phase. To the contrary, Refs. [20,21] have recently developed another calculus, in which the two chemical potentials are calculated directly from the other intensive quantities of the system, temperature or pressure, baryon density and isospin asymmetry. In the present paper we extend the works [20,21] to the generalized thermo-statistics.

Our formulation of warm nuclear matter is essentially based on Ref. [11], which investigates isospin symmetric matter in the generalized thermo-statistics. Its application to asymmetric matter is straightforward. Using the q-deformed exponential and logarithm

$$\exp_q(x) \equiv [\,1 + (1-q)\,x\,]^{1/(1-q)}\,, \tag{1}$$

$$\ln_q(x) \equiv \frac{x^{1-q}-1}{1-q}, \tag{2}$$

the thermodynamic potential per volume is given by

$$\begin{aligned}\Omega &= \frac{1}{2}\,m_\sigma^2\,\langle\sigma\rangle^2 + \frac{1}{2}\,m_\delta^2\,\langle\delta_3\rangle^2 - \frac{1}{2}\,m_\omega^2\,\langle\omega_0\rangle^2 - \frac{1}{2}\,m_\rho^2\,\langle\rho_{03}\rangle^2 \\ &\quad - \gamma\,k_B\tau \sum_{i=p,n}\int \frac{d^3\mathbf{k}}{(2\pi)^3}\ln_q\left[1+\exp_q\left(\frac{\nu_i - E_{ki}^*}{k_B\tau}\right)\right],\end{aligned} \tag{3}$$

where q is the power-law index, $\gamma = 2$ is the spin degeneracy factor, k_B is the Boltzmann constant and ν_i is defined using the chemical potential μ_i and the vector potential V_i as

$$\nu_i = \mu_i - V_i. \tag{4}$$

$E_{ki}^* = \left(\mathbf{k}^2 + M_i^{*2}\right)^{1/2}$ is the energy of nucleon. We have neglected the effect of anti-nucleon. Moreover, it is noted [22,24] that τ is not physical intensive temperature but $1/\left(k_B\tau\right)$ is only the Lagrange multiplier associated with the extremalization of an entropic measure.

We have used the relativistic mean-field model [23] to describe nuclear matter. The effective masses $M_{p(n)}^* = m_{p(n)}^* M_N$ and the vector potentials $V_{p(n)} = v_{p(n)} M_N$ are determined by extremizing Ω:

$$\begin{aligned}\frac{\partial\,\Omega}{\partial M_p^*} &= \rho_{Sp} + m_\sigma^2\,\frac{\langle\sigma\rangle}{M_N}\,\frac{\partial\,\langle\sigma\rangle}{\partial\,m_p^*} + m_\delta^2\,\frac{\langle\delta_3\rangle}{M_N}\,\frac{\partial\,\langle\delta_3\rangle}{\partial\,m_p^*} \\ &\quad - m_\omega^2\,\frac{\langle\omega_0\rangle}{M_N}\,\frac{\partial\,\langle\omega_0\rangle}{\partial\,m_p^*} - m_\rho^2\,\frac{\langle\rho_{03}\rangle}{M_N}\,\frac{\partial\,\langle\rho_{03}\rangle}{\partial\,m_p^*} \;=\; 0,\end{aligned} \tag{5}$$

$$\begin{aligned}\frac{\partial\,\Omega}{\partial V_p} &= \rho_{Bp} + m_\sigma^2\,\frac{\langle\sigma\rangle}{M_N}\,\frac{\partial\,\langle\sigma\rangle}{\partial\,v_p} + m_\delta^2\,\frac{\langle\delta_3\rangle}{M_N}\,\frac{\partial\,\langle\delta_3\rangle}{\partial\,v_p} \\ &\quad - m_\omega^2\,\frac{\langle\omega_0\rangle}{M_N}\,\frac{\partial\,\langle\omega_0\rangle}{\partial\,v_p} - m_\rho^2\,\frac{\langle\rho_{03}\rangle}{M_N}\,\frac{\partial\,\langle\rho_{03}\rangle}{\partial\,v_p} \;=\; 0,\end{aligned} \tag{6}$$

$$\begin{aligned}\frac{\partial\,\Omega}{\partial M_n^*} &= \rho_{Sn} + m_\sigma^2\,\frac{\langle\sigma\rangle}{M_N}\,\frac{\partial\,\langle\sigma\rangle}{\partial\,m_n^*} + m_\delta^2\,\frac{\langle\delta_3\rangle}{M_N}\,\frac{\partial\,\langle\delta_3\rangle}{\partial\,m_n^*} \\ &\quad - m_\omega^2\,\frac{\langle\omega_0\rangle}{M_N}\,\frac{\partial\,\langle\omega_0\rangle}{\partial\,m_n^*} - m_\rho^2\,\frac{\langle\rho_{03}\rangle}{M_N}\,\frac{\partial\,\langle\rho_{03}\rangle}{\partial\,m_n^*} \;=\; 0,\end{aligned} \tag{7}$$

$$\begin{aligned}\frac{\partial\,\Omega}{\partial V_n} &= \rho_{Bn} + m_\sigma^2\,\frac{\langle\sigma\rangle}{M_N}\,\frac{\partial\,\langle\sigma\rangle}{\partial\,v_n} + m_\delta^2\,\frac{\langle\delta_3\rangle}{M_N}\,\frac{\partial\,\langle\delta_3\rangle}{\partial\,v_n} \\ &\quad - m_\omega^2\,\frac{\langle\omega_0\rangle}{M_N}\,\frac{\partial\,\langle\omega_0\rangle}{\partial\,v_n} - m_\rho^2\,\frac{\langle\rho_{03}\rangle}{M_N}\,\frac{\partial\,\langle\rho_{03}\rangle}{\partial\,v_n} \;=\; 0,\end{aligned} \tag{8}$$

where the mean-fields are expressed [23] in terms of the effective masses and the vector potentials. The explicit expressions of the derivatives of mean fields are also given in Ref. [23]. The baryon and scalar densities are defined by [11,24]

$$\rho_{Bi} = \gamma \int \frac{d^3\mathbf{k}}{(2\pi)^3} \left[n_i \left(m_i^*, v_i, \mu_i, \tau, q, k \right) \right]^q, \tag{9}$$

$$\rho_{Si} = \gamma \int \frac{d^3\mathbf{k}}{(2\pi)^3} \frac{M_i^*}{E_{ki}^*} \left[n_i \left(m_i^*, v_i, \mu_i, \tau, q, k \right) \right]^q, \tag{10}$$

where the q-deformed Fermi-Dirac distribution function is [11,24]

$$n_i \left(m_i^*, v_i, \mu_i, \tau, q, k \right) = \begin{cases} \dfrac{1}{1 + \left[1 + (q-1) \frac{E_{ki}^* - \nu_i}{k_B \tau} \right]^{\frac{1}{q-1}}} & \text{for} \quad 1 + (q-1) \dfrac{E_{ki}^* - \nu_i}{k_B \tau} > 0, \\ 1 & \text{for} \quad 1 + (q-1) \dfrac{E_{ki}^* - \nu_i}{k_B \tau} \leq 0. \end{cases} \tag{11}$$

The q-deformed Fermi integrals are calculated using the adaptive automatic integration with 20-points Gaussian quadrature.

It is noted [22] that the phase equilibrium should be defined in terms of intensive temperature T and conjugate extensive entropy S. Here, they are introduced through the Gibbs thermodynamic relation [11]:

$$\Omega = U - TS - \left(\mu_p \rho_{Bp} + \mu_n \rho_{Bn} \right), \tag{12}$$

where the energy density U is

$$\begin{aligned} U &= \frac{1}{2} m_\sigma^2 \langle \sigma \rangle^2 + \frac{1}{2} m_\delta^2 \langle \delta_3 \rangle^2 - \frac{1}{2} m_\omega^2 \langle \omega_0 \rangle^2 - \frac{1}{2} m_\rho^2 \langle \rho_{03} \rangle^2 \\ &\quad + \gamma \sum_{i=p,n} \int \frac{d^3\mathbf{k}}{(2\pi)^3} E_{ki}^* \left[n_i \left(m_i^*, v_i, \mu_i, \tau, q, k \right) \right]^q + \sum_{i=p,n} V_i \, \rho_{Bi}. \end{aligned} \tag{13}$$

Because of Eq. (12), T and S are determined from a single thermodynamic quantity. In practice, according to the mapping of Tsallis non-extensive thermo-statistics on the standard Boltzmann-Gibbs thermo-statistics [25-27], they are expressed by the Tsallis non-extensive entropy S_q:

$$T = C_q \, \tau, \tag{14}$$

$$\frac{S}{\rho_B} = \frac{\ln C_q}{1-q}, \tag{15}$$

where

$$C_q = 1 + (1-q) \, S_q, \tag{16}$$

$$\rho_B = \rho_{Bp} + \rho_{Bn}. \tag{17}$$

In order to guarantee $C_q > 0$ we assume [11] that the power-law index depends on the baryon density:

$$q - 1 = \frac{1}{3} \frac{\rho_B/\rho_0}{\rho_B/\rho_0 + 2}, \tag{18}$$

where $\rho_0 = 0.16\text{fm}^{-3}$ is the saturation density of symmetric nuclear matter. The density dependence is constrained from the condition

$$1 < q < 4/3. \tag{19}$$

This is necessary [11] for the relation $P = -\Omega$, where P is the pressure density,

$$\begin{aligned} P &= \frac{\gamma}{3} \sum_{i=p,n} \int \frac{d^3\mathbf{k}}{(2\pi)^3} \frac{k^2}{E^*_{ki}} \left[n_i \left(m^*_i, v_i, \mu_i, \tau, q, k \right) \right]^q \\ &\quad - \frac{1}{2} m^2_\sigma \langle \sigma \rangle^2 - \frac{1}{2} m^2_\delta \langle \delta_3 \rangle^2 + \frac{1}{2} m^2_\omega \langle \omega_0 \rangle^2 + \frac{1}{2} m^2_\rho \langle \rho_{03} \rangle^2 . \end{aligned} \tag{20}$$

Moreover, the condition (19) guarantees [11] finite values of the q-deformed Fermi integrals in Eqs. (9), (10), (13) and (20).

For definite values of physical intensive temperature T, baryon density ρ_B and isospin asymmetry

$$a = \frac{\rho_{Bn} - \rho_{Bp}}{\rho_{Bn} + \rho_{Bp}}, \tag{21}$$

we solve 7th-rank nonlinear simultaneous equations (5)-(8), (12), (17) and (21) using the globally convergent Newton-Raphson algorithm [28] so that the effective masses, the vector potentials, the chemical potentials and the non-extensive entropy are determined. The pressure density, the energy density and the extensive entropy are also determined at a time.

The black curves in Figs. 1 and 2 show the solutions of chemical potentials for $T = 10\text{MeV}$ and $a = 0.3$ as functions of pressure. (We set the Boltzmann constant as unit.) The black curves in Fig. 3 show the pressure-density isotherms for several asymmetries. They exhibit typical nature of van der Waals equation-of-state. The solid parts on lower pressure and density are the branches for pure gas phase while the solid parts on higher pressure and density are the branches for pure liquid phase. The dashed parts correspond to the liquid-gas phase transition. They are not however realized because the Gibbs condition on phase equilibrium is not satisfied. In fact, as the nuclear matter is compressed in Figs. 1 and 2, we cannot reach to the liquid branches from the gas branches.

So as to construct the physically reasonable liquid-gas mixed phase being consistent with the Gibbs condition on phase equilibrium, we have to solve the following 15th-rank simultaneous nonlinear equations. The four equations of them determine the effective masses and the vector potentials of proton and neutron in gaseous phase:

$$\frac{\partial\,\Omega}{\partial M_p^{(g)*}} = \rho_{Sp}^{(g)} + m_\sigma^2\,\frac{\langle\sigma\rangle_g}{M_N}\,\frac{\partial\,\langle\sigma\rangle_g}{\partial\,m_p^{(g)*}} + m_\delta^2\,\frac{\langle\delta_3\rangle_g}{M_N}\,\frac{\partial\,\langle\delta_3\rangle_g}{\partial\,m_p^{(g)*}} - m_\omega^2\,\frac{\langle\omega_0\rangle_g}{M_N}\,\frac{\partial\,\langle\omega_0\rangle_g}{\partial\,m_p^{(g)*}} - m_\rho^2\,\frac{\langle\rho_{03}\rangle_g}{M_N}\,\frac{\partial\,\langle\rho_{03}\rangle_g}{\partial\,m_p^{(g)*}} \;=\; 0, \tag{22}$$

$$\frac{\partial\,\Omega}{\partial V_p^{(g)}} = \rho_{Bp}^{(g)} + m_\sigma^2\,\frac{\langle\sigma\rangle_g}{M_N}\,\frac{\partial\,\langle\sigma\rangle_g}{\partial\,v_p^{(g)}} + m_\delta^2\,\frac{\langle\delta_3\rangle_g}{M_N}\,\frac{\partial\,\langle\delta_3\rangle_g}{\partial\,v_p^{(g)}} - m_\omega^2\,\frac{\langle\omega_0\rangle_g}{M_N}\,\frac{\partial\,\langle\omega_0\rangle_g}{\partial\,v_p^{(g)}} - m_\rho^2\,\frac{\langle\rho_{03}\rangle_g}{M_N}\,\frac{\partial\,\langle\rho_{03}\rangle_g}{\partial\,v_p^{(g)}} \;=\; 0, \tag{23}$$

$$\frac{\partial\,\Omega}{\partial M_n^{(g)*}} = \rho_{Sn}^{(g)} + m_\sigma^2\,\frac{\langle\sigma\rangle_g}{M_N}\,\frac{\partial\,\langle\sigma\rangle_g}{\partial\,m_n^{(g)*}} + m_\delta^2\,\frac{\langle\delta_3\rangle_g}{M_N}\,\frac{\partial\,\langle\delta_3\rangle_g}{\partial\,m_n^{(g)*}} - m_\omega^2\frac{\langle\omega_0\rangle_g}{M_N}\frac{\partial\,\langle\omega_0\rangle_g}{\partial\,m_n^{(g)*}} - m_\rho^2\frac{\langle\rho_{03}\rangle_g}{M_N}\frac{\partial\,\langle\rho_{03}\rangle_g}{\partial\,m_n^{(g)*}} \;=\; 0, \tag{24}$$

$$\frac{\partial\,\Omega}{\partial V_n^{(g)}} = \rho_{Bn}^{(g)} + m_\sigma^2\,\frac{\langle\sigma\rangle_g}{M_N}\,\frac{\partial\,\langle\sigma\rangle_g}{\partial\,v_n^{(g)}} + m_\delta^2\,\frac{\langle\delta_3\rangle_g}{M_N}\,\frac{\partial\,\langle\delta_3\rangle_g}{\partial\,v_n^{(g)}} - m_\omega^2\,\frac{\langle\omega_0\rangle_g}{M_N}\,\frac{\partial\,\langle\omega_0\rangle_g}{\partial\,v_n^{(g)}} - m_\rho^2\,\frac{\langle\rho_{03}\rangle_g}{M_N}\,\frac{\partial\,\langle\rho_{03}\rangle_g}{\partial\,v_n^{(g)}} \;=\; 0, \tag{25}$$

where the suffix g indicates gaseous phase. It is noted again that the mean-fields are expressed in terms of the effective masses and the vector potentials. Similarly, the equations for liquid phase are

$$\frac{\partial\,\Omega}{\partial M_p^{(l)*}} = \rho_{Sp}^{(l)} + m_\sigma^2\,\frac{\langle\sigma\rangle_l}{M_N}\,\frac{\partial\,\langle\sigma\rangle_l}{\partial\,m_p^{(l)*}} + m_\delta^2\,\frac{\langle\delta_3\rangle_l}{M_N}\,\frac{\partial\,\langle\delta_3\rangle_l}{\partial\,m_p^{(l)*}} - m_\omega^2\,\frac{\langle\omega_0\rangle_l}{M_N}\,\frac{\partial\,\langle\omega_0\rangle_l}{\partial\,m_p^{(l)*}} - m_\rho^2\,\frac{\langle\rho_{03}\rangle_l}{M_N}\,\frac{\partial\,\langle\rho_{03}\rangle_l}{\partial\,m_p^{(l)*}} \;=\; 0, \tag{26}$$

$$\frac{\partial\,\Omega}{\partial V_p^{(l)}} = \rho_{Bp}^{(l)} + m_\sigma^2\,\frac{\langle\sigma\rangle_l}{M_N}\,\frac{\partial\,\langle\sigma\rangle_l}{\partial\,v_p^{(l)}} + m_\delta^2\,\frac{\langle\delta_3\rangle_l}{M_N}\,\frac{\partial\,\langle\delta_3\rangle_l}{\partial\,v_p^{(l)}} - m_\omega^2\,\frac{\langle\omega_0\rangle_l}{M_N}\,\frac{\partial\,\langle\omega_0\rangle_l}{\partial\,v_p^{(l)}} - m_\rho^2\,\frac{\langle\rho_{03}\rangle_l}{M_N}\,\frac{\partial\,\langle\rho_{03}\rangle_l}{\partial\,v_p^{(l)}} \;=\; 0, \tag{27}$$

$$\frac{\partial\,\Omega}{\partial M_n^{(l)*}} = \rho_{Sn}^{(l)} + m_\sigma^2\,\frac{\langle\sigma\rangle_l}{M_N}\,\frac{\partial\,\langle\sigma\rangle_l}{\partial\,m_n^{(l)*}} + m_\delta^2\,\frac{\langle\delta_3\rangle_l}{M_N}\,\frac{\partial\,\langle\delta_3\rangle_l}{\partial\,m_n^{(l)*}} - m_\omega^2\,\frac{\langle\omega_0\rangle_l}{M_N}\,\frac{\partial\,\langle\omega_0\rangle_l}{\partial\,m_n^{(l)*}} - m_\rho^2\,\frac{\langle\rho_{03}\rangle_l}{M_N}\,\frac{\partial\,\langle\rho_{03}\rangle_l}{\partial\,m_n^{(l)*}} = 0, \tag{28}$$

$$\frac{\partial\,\Omega}{\partial V_n^{(l)}} = \rho_{Bn}^{(l)} + m_\sigma^2\,\frac{\langle\sigma\rangle_l}{M_N}\,\frac{\partial\,\langle\sigma\rangle_l}{\partial\,v_n^{(l)}} + m_\delta^2\,\frac{\langle\delta_3\rangle_l}{M_N}\,\frac{\partial\,\langle\delta_3\rangle_l}{\partial\,v_n^{(l)}} - m_\omega^2\,\frac{\langle\omega_0\rangle_l}{M_N}\,\frac{\partial\,\langle\omega_0\rangle_l}{\partial\,v_n^{(l)}} - m_\rho^2\,\frac{\langle\rho_{03}\rangle_l}{M_N}\,\frac{\partial\,\langle\rho_{03}\rangle_l}{\partial\,v_n^{(l)}} = 0. \tag{29}$$

The other two equations specify the densities of proton and neutron in liquid-gas mixed phase:

$$\rho_{Bp} = \frac{1}{2}\,(1-a)\,\rho_B = f_g\,\rho_{Bp}^{(g)} + (1-f_g)\,\rho_{Bp}^{(l)}, \tag{30}$$

$$\rho_{Bn} = \frac{1}{2}\,(1+a)\,\rho_B = f_g\,\rho_{Bn}^{(g)} + (1-f_g)\,\rho_{Bn}^{(l)}, \tag{31}$$

where $0 \le f_g \le 1$ is the ratio of gas. The baryon densities in gaseous and liquid phases are

$$\rho_{Bi}^{(g)} = \gamma \int \frac{d^3\mathbf{k}}{(2\pi)^3}\left[\,n_i\left(m_i^{(g)*}, v_i^{(g)}, \mu_i, \tau_g, q_g, k\right)\right]^q, \tag{32}$$

$$\rho_{Bi}^{(l)} = \gamma \int \frac{d^3\mathbf{k}}{(2\pi)^3}\left[\,n_i\left(m_i^{(l)*}, v_i^{(l)}, \mu_i, \tau_l, q_l, k\right)\right]^q. \tag{33}$$

It is noted that the virtual temperature τ is not equilibrated. The power-law indices in gaseous and liquid phases are also determined self-consistently because they depend on each density of the two phases:

$$q_g - 1 = \frac{1}{3}\,\frac{\left(\rho_{Bp}^{(g)} + \rho_{Bn}^{(g)}\right)/\rho_0}{\left(\rho_{Bp}^{(g)} + \rho_{Bn}^{(g)}\right)/\rho_0 + 2}, \tag{34}$$

$$q_l - 1 = \frac{1}{3}\,\frac{\left(\rho_{Bp}^{(l)} + \rho_{Bn}^{(l)}\right)/\rho_0}{\left(\rho_{Bp}^{(l)} + \rho_{Bn}^{(l)}\right)/\rho_0 + 2}. \tag{35}$$

Moreover, we have to assume the thermodynamic relations in gaseous and liquid phases:

$$P_g + U_g - TS_g - \left(\mu_p\rho_{Bp}^{(g)} + \mu_n\rho_{Bn}^{(g)}\right) = 0, \tag{36}$$

$$P_l + U_l - TS_l - \left(\mu_p\rho_{Bp}^{(l)} + \mu_n\rho_{Bn}^{(l)}\right) = 0, \tag{37}$$

where

$$U_g = \frac{1}{2} m_\sigma^2 \langle\sigma\rangle_g^2 + \frac{1}{2} m_\delta^2 \langle\delta_3\rangle_g^2 - \frac{1}{2} m_\omega^2 \langle\omega_0\rangle_g^2 - \frac{1}{2} m_\rho^2 \langle\rho_{03}\rangle_g^2 + \gamma \sum_{i=p,n} \int \frac{d^3\mathbf{k}}{(2\pi)^3} E_{ki}^{(g)*} \left[n_i \left(m_i^{(g)*}, v_i^{(g)}, \mu_i, \tau_g, q_g, k \right) \right]^q + \sum_{i=p,n} V_i^{(g)} \rho_{Bi}^{(g)}, \quad (38)$$

$$U_l = \frac{1}{2} m_\sigma^2 \langle\sigma\rangle_l^2 + \frac{1}{2} m_\delta^2 \langle\delta_3\rangle_l^2 - \frac{1}{2} m_\omega^2 \langle\omega_0\rangle_l^2 - \frac{1}{2} m_\rho^2 \langle\rho_{03}\rangle_l^2 + \gamma \sum_{i=p,n} \int \frac{d^3\mathbf{k}}{(2\pi)^3} E_{ki}^{(l)*} \left[n_i \left(m_i^{(l)*}, v_i^{(l)}, \mu_i, \tau_l, q_l, k \right) \right]^q + \sum_{i=p,n} V_i^{(l)} \rho_{Bi}^{(l)}. \quad (39)$$

The last equation imposes the equilibrium condition on pressures in the two phases:

$$\begin{aligned} P_g &\equiv \frac{\gamma}{3} \sum_{i=p,n} \int \frac{d^3\mathbf{k}}{(2\pi)^3} \frac{k^2}{E_{ki}^{(g)*}} \left[n_i \left(m_i^{(g)*}, v_i^{(g)}, \mu_i, \tau_g, q_g, k \right) \right]^q \\ &\quad - \frac{1}{2} m_\sigma^2 \langle\sigma\rangle_g^2 - \frac{1}{2} m_\delta^2 \langle\delta_3\rangle_g^2 + \frac{1}{2} m_\omega^2 \langle\omega_0\rangle_g^2 + \frac{1}{2} m_\rho^2 \langle\rho_{03}\rangle_g^2 \\ &= P_l \equiv \frac{\gamma}{3} \sum_{i=p,n} \int \frac{d^3\mathbf{k}}{(2\pi)^3} \frac{k^2}{E_{ki}^{(l)*}} \left[n_i \left(m_i^{(l)*}, v_i^{(l)}, \mu_i, \tau_l, q_l, k \right) \right]^q \\ &\quad - \frac{1}{2} m_\sigma^2 \langle\sigma\rangle_l^2 - \frac{1}{2} m_\delta^2 \langle\delta_3\rangle_l^2 + \frac{1}{2} m_\omega^2 \langle\omega_0\rangle_l^2 + \frac{1}{2} m_\rho^2 \langle\rho_{03}\rangle_l^2 . \end{aligned} \quad (40)$$

Solving Eqs. (22)-(31), (34)-(37) and (40) for definite values of temperature T, baryon density ρ_B and isospin asymmetry a, we have the effective masses, the vector potentials, the non-extensive entropies and the power-law indices in gaseous and liquid phases as well as the chemical potentials and the ratio of gas (or liquid) phase. The baryon and energy densities in the two phases and the equilibrated pressure are also determined at a time. The total entropy is given by $f_g S_g + (1 - f_g) S_l$ because S_g and S_l are the extensive entropies. The total energy density is also given by $U = f_g U_g + (1 - f_g) U_l$.

The solutions of chemical potentials for $T = 10$MeV and $a = 0.3$ are shown by the red curves in Figs. 1 and 2. As the nuclear matter is compressed between $P = 0.049$MeV/fm^3 and 0.091MeV/fm^3, μ_p decreases while μ_n increases. The results indicate that the ratios of neutron increase in both of liquid and gaseous phases. This is clearly seen in Fig. 4, where the asymmetry $a_g = \frac{\left(\rho_{Bn}^{(g)} - \rho_{Bp}^{(g)}\right)}{\left(\rho_{Bn}^{(g)} + \rho_{Bp}^{(g)}\right)}$ in gaseous phase and the asymmetry $a_l = \frac{\left(\rho_{Bn}^{(l)} - \rho_{Bp}^{(l)}\right)}{\left(\rho_{Bn}^{(l)} + \rho_{Bp}^{(l)}\right)}$ in liquid phase are shown by the red and blue curves, respectively. The ratio of liquid phase $f_l = 1.0 - f_g$ is also shown by the black curve. Moreover, we see in Figs. 1 and 2 that $\partial\mu_p/\partial P$ and $\partial\mu_n/\partial P$ have discontinuities at the beginning and ending points of the phase transition. It is therefore concluded [11] that the phase transition is the first order.

The pressure-density isotherms in the phase transition are also shown by the red curves in Fig. 3. As the asymmetry becomes higher, the nuclear matter is compressed more weakly while a gain of pressure is larger. The liquid-gas mixed phase for $a = 0.5$

is not shown because above some baryon density we have no solutions of Eqs. (22)-(31), (34)-(37) and (40). The problem is revealed more generally in the binodal surface of Fig. 5. The red and blue curves are gas and liquid branches. The former ends at $a = 0.84$ while the latter ends at $a = 0.42$. Consequently, there is no critical point, on which the two branches connect with each other except for equal concentration $a = 0$. The absence of critical point is essentially due to the effective density-dependent nucleon-nucleon interaction. In practice, it has been also found [15,19,20] in the standard thermo-statistics. However, there are differences between the standard and generalized thermo-statistics. The region of no gas and liquid branches between $a = 0.42$ and 0.84 is much wider than those in Refs. [15,19,20]. Moreover, the gas branch in Fig. 5 does not show the retrograde condensation predicted in Refs. [14-20].

Next, we investigate the thermodynamic properties of nuclear matter for definite values of pressure P, baryon density ρ_B and isospin asymmetry a. Solving 7th-rank nonlinear simultaneous equations (5)-(8), (17), (20) and (21), the effective masses, the vector potentials, the chemical potentials and the virtual temperature τ are determined. The energy density is also determined at a time. The physical temperature T is calculated from a variation of Eq. (12):

$$\frac{T \ln (T/\tau)}{1-q} = \frac{U + P - \left(\mu_p \rho_{Bp} + \mu_n \rho_{Bn}\right)}{\rho_B}. \tag{41}$$

Then, the extensive entropy is calculated from Eq. (15).

The black curves in Figs. 6 and 7 show the solutions of chemical potentials for $P = 0.03\mathrm{MeV/fm}^3$ and $a = 0.3$ as functions of temperature T. The solid parts on lower temperature are the branches for pure liquid phase while the solid parts on higher temperature are the branches for pure gas phase. The dashed parts correspond to the liquid-gas phase transition. The black curve in Fig. 8 shows the caloric curve, the temperature as a function of the excitation energy per particle, which is defined by subtracting the binding energy of cold asymmetric nuclear matter [23] from U/ρ_B. The solid part is the pure liquid phase while the dashed part is the liquid-gas mixed phase. The triangles are the experimental data of Fig. 5 in Ref. [29]. The black dashed curves in Figs. 6-8 are not realized because the Gibbs condition on phase equilibrium is not satisfied. In fact, as the nuclear matter is heated in Figs. 6 and 7, we cannot reach to the gas branches from the liquid branches.

So as to construct the physically reasonable liquid-gas mixed phase being consistent with the Gibbs condition on phase equilibrium, for definite values of pressure P, baryon density ρ_B and isospin asymmetry a, we have to solve 16th-rank simultaneous nonlinear equations (22)-(31), (34), (35), the thermodynamic relations in gaseous and liquid phases,

$$P + U_g - TS_g - \left(\mu_p \rho_{Bp}^{(g)} + \mu_n \rho_{Bn}^{(g)}\right) = 0, \tag{42}$$

$$P + U_l - TS_l - \left(\mu_p \rho_{Bp}^{(l)} + \mu_n \rho_{Bn}^{(l)}\right) = 0, \tag{43}$$

and the equilibrium conditions on pressures in the two phases,

$$\begin{aligned} P &= \frac{\gamma}{3} \sum_{i=p,n} \int \frac{d^3\mathbf{k}}{(2\pi)^3} \frac{k^2}{E_{ki}^{(g)*}} \left[n_i \left(m_i^{(g)*}, v_i^{(g)}, \mu_i, \tau_g, q_g, k \right) \right]^q \\ &\quad - \frac{1}{2} m_\sigma^2 \langle\sigma\rangle_g^2 - \frac{1}{2} m_\delta^2 \langle\delta_3\rangle_g^2 + \frac{1}{2} m_\omega^2 \langle\omega_0\rangle_g^2 + \frac{1}{2} m_\rho^2 \langle\rho_{03}\rangle_g^2 , \end{aligned} \tag{44}$$

$$\begin{aligned} P &= \frac{\gamma}{3} \sum_{i=p,n} \int \frac{d^3\mathbf{k}}{(2\pi)^3} \frac{k^2}{E_{ki}^{(l)*}} \left[n_i \left(m_i^{(l)*}, v_i^{(l)}, \mu_i, \tau_l, q_l, k \right) \right]^q \\ &\quad - \frac{1}{2} m_\sigma^2 \langle\sigma\rangle_l^2 - \frac{1}{2} m_\delta^2 \langle\delta_3\rangle_l^2 + \frac{1}{2} m_\omega^2 \langle\omega_0\rangle_l^2 + \frac{1}{2} m_\rho^2 \langle\rho_{03}\rangle_l^2 . \end{aligned} \tag{45}$$

We have the effective masses, the vector potentials, the non-extensive entropies and the power-law indices in gaseous and liquid phases as well as the chemical potentials, the ratio of gas (or liquid) phase and the internal physical temperature. The energy densities in the two phases are also determined at a time.

The solutions of chemical potentials for $P = 0.03\text{MeV/fm}^3$ and $a = 0.3$ are shown by the red curves in Figs. 6 and 7. As the nuclear matter is heated from $T = 5.79\text{MeV}$ to 8.80MeV, μ_p increases while μ_n decreases. The results indicate that the ratios of neutron decrease in both of liquid and gaseous phases. This is clearly seen in Fig. 9, where the asymmetries in the two phases are shown by the red and blue curves, respectively. The ratio of liquid $f_l = 1.0 - f_g$ is also shown by the black curve. The boiling of nuclear liquid under constant pressure is shown more generally in Fig. 10, where the blue and red curves are the boiling temperature of nuclear liquid and the condensed temperature of nuclear gas, respectively. The dotted lines indicate that the nuclear liquid of asymmetry $a = 0.3$ begins to evaporate into highly asymmetric nuclear gas of $a_g = 0.977$, which is almost composed of neutrons. When the evaporation completes, the liquid phase is in rather symmetric state of asymmetry $a_l = 0.057$. The caloric curve in liquid-gas phase transition is also shown by the red curve in Fig. 8. It reproduces the experimental data better than the black dashed curve. Consequently, we can see that the experimental data provide the clear evidence of nuclear liquid-gas phase transition.

The liquid-gas phase transition in asymmetric nuclear matter has been investigated for the first time within the generalized thermo-statistics. A new calculus of the phase transition in the standard thermo-statistics is applicable to the generalized thermo-statistics. We however have to solve higher-order simultaneous nonlinear equations than those in the standard thermo-statistics. This is because the phase equilibrium can be defined only in terms of intensive temperature and conjugate extensive entropy. So as to determine them the Gibbs thermodynamic relation should be imposed on the thermodynamic

potential. Moreover, the power-law index depends on the baryon density so that the extensive entropy is not negative.

We have investigated the isothermal compression and the boiling under constant pressure. The essential features of nuclear liquid-gas phase transition in the generalized thermo-statistics are similar to those in the standard thermo-statistics. The derivatives of chemical potentials have discontinuities at the ends of phase transition. We can therefore conclude that the phase transition is the first order. The liquid and gas branches in the section of binodal surface are connected with each other only on the equal concentration, but there is no critical point. The caloric curve calculated for appropriate values of asymmetry and pressure reproduces the experimental data well. We however cannot find the retrograde condensation predicted in the standard thermo-statistics.

References

[1] C. Tsallis, Braz. J. Phys. **29** (1999) 1.

[2] Europhysics News **36** (2005) No.6 [http://www.europhysicsnews.com].

[3] V.E. Viola *et al.*, Phys. Rep. **434** (2006) 1 [arXiv:nucl-ex/0604012].

[4] V.A. Karnaukhov, Phys. Elem. Part. Atom. Nucl. **37** (2006) 312 [http://www1.jinr.ru/Pepan/Pepan_index.html].

[5] D.B. Walton and J. Rafelski, Phys. Rev. Lett. **84** (2000) 31 [arXiv:hep-ph/9907273].

[6] K.K. Gudima, A.S. Parvan, M. Płoszajczak and V.D. Toneev, Phys. Rev. Lett. **84** (2000) 4691 [arXiv:nucl-th/0003025].

[7] C.E. Aguiar and T. Kodama, Physica A **320** (2003) 371.

[8] A. Drago, A. Lavagno and P. Quarati, Physica A **344** (2004) 472 [arXiv:nucl-th/0312108].

[9] F.I.M. Pereira, R. Silva and J.S. Alcaniz, Phys. Rev. C **76** (2007) 015201 [arXiv:nucl-th/0705.0300].

[10] T. Osada and G. Wilk, arXiv:nucl-th/0710.1905.

[11] K. Miyazaki, Mathematical Physics Preprint Archive (mp_arc) 07-230.

[12] J. Richert and P. Wagner, Phys. Rep. **350** (2001) 1 [arXiv:nucl-th/0009023].

[13] S.D. Gupta, A.Z. Mekjian and M.B. Tsang, *Advances in Nuclear Physics*, Vol. **26** (Kluwer Academic, 2001) [arXiv:nucl-th/0009033].

[14] H. Müller and B. D. Serot, Phys. Rev. C **52** (1995) 2072 [arXiv:nucl-th/9505013].

[15] W.L. Qian, R-K. Su and P. Wang, Phys. Lett. B **491** (2000) 90 [arXiv:nucl-th/0008057].

[16] V.M. Kolomietz, A.I. Sanzhur, S. Shlomo and S.A. Firin, Phys. Rev. C **64** (2001) 024315 [arXiv:nucl-th/0104013].

[17] P.K. Panda, G. Klein, D.P. Menezes and C. Providência, Phys. Rev. C **68** (2003) 015201 [arXiv:nucl-th/0306045].

[18] P. Wang, D.B. Leinweber, A.W. Thomas and A.G. Williams, Nucl. Phys. A **748** (2005) 226 [arXiv:nucl-th/0407057].

[19] J. Xu. L-W. Chen, B-A. Li and H-R. Ma, Phys. Lett. B **650** (2007) 348 [arXiv:nucl-th/0702085].

[20] K. Miyazaki, Mathematical Physics Preprint Archive (mp_arc) 07-92.

[21] K. Miyazaki, Mathematical Physics Preprint Archive (mp_arc) 07-141.

[22] S. Abe, S. Martínez, F. Pennini and A. Plastino, Phys. Lett. A **281** (2001) 126 [arXiv:cond-mat/0011012].

[23] K. Miyazaki, Mathematical Physics Preprint Archive (mp_arc) 06-336.

[24] A.M. Teweldeberhan, A.R. Plastino and H.G. Miller, Phys. Lett. A **343** (2005) 71. [arXiv:cond-mat/0504516].

[25] E. Vives and A. Planes, Phys. Rev. Lett. **88** (2002) 020601 [arXiv:cond-mat/0106428].

[26] R. Toral, Physica A **317** (2003) 209.

[27] A.S. Parvan, Phys. Lett. A **350** (2006) 331 [arXiv:cond-mat/0506392].

[28] W.H. Press, S.A. Teukolsky, W.T. Vetterling and B.P. Flannery, Numerical Recipes in C 2nd edition, 1992, Cambridge University Press, [http://www.nr.com/].

[29] A. Ruangma *et al.*, Phys. Rev. C **66** (2002) 044603.

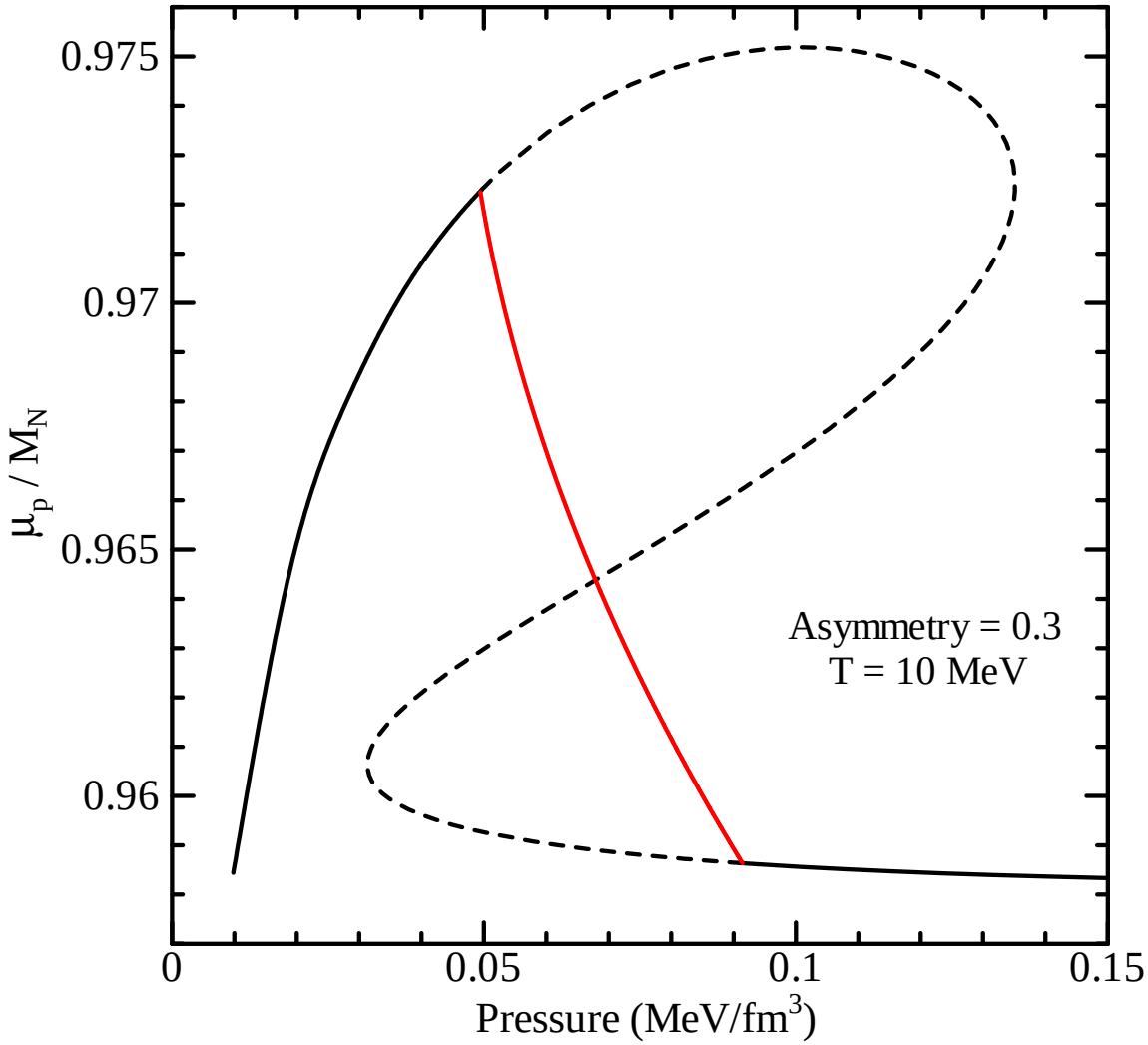

Figure 1: The proton chemical potential as a function of pressure for $T = 10$MeV and $a = 0.3$. The black dashed curve does not satisfy the Gibbs condition on phase equilibrium while the physically precise liquid-gas phase transition is expressed by the red curve.

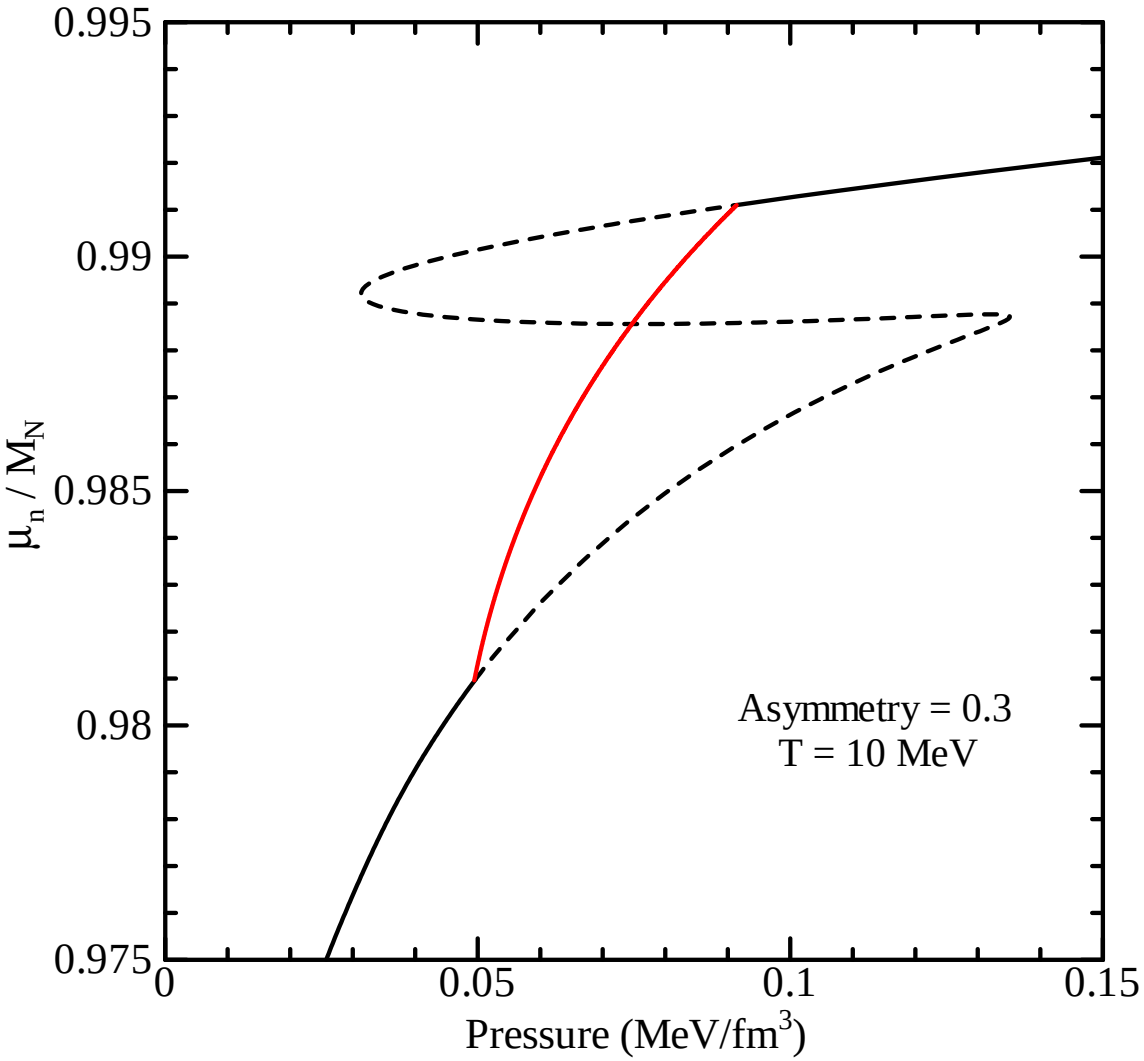

Figure 2: The same as Fig. 1 but for neutron chemical potential.

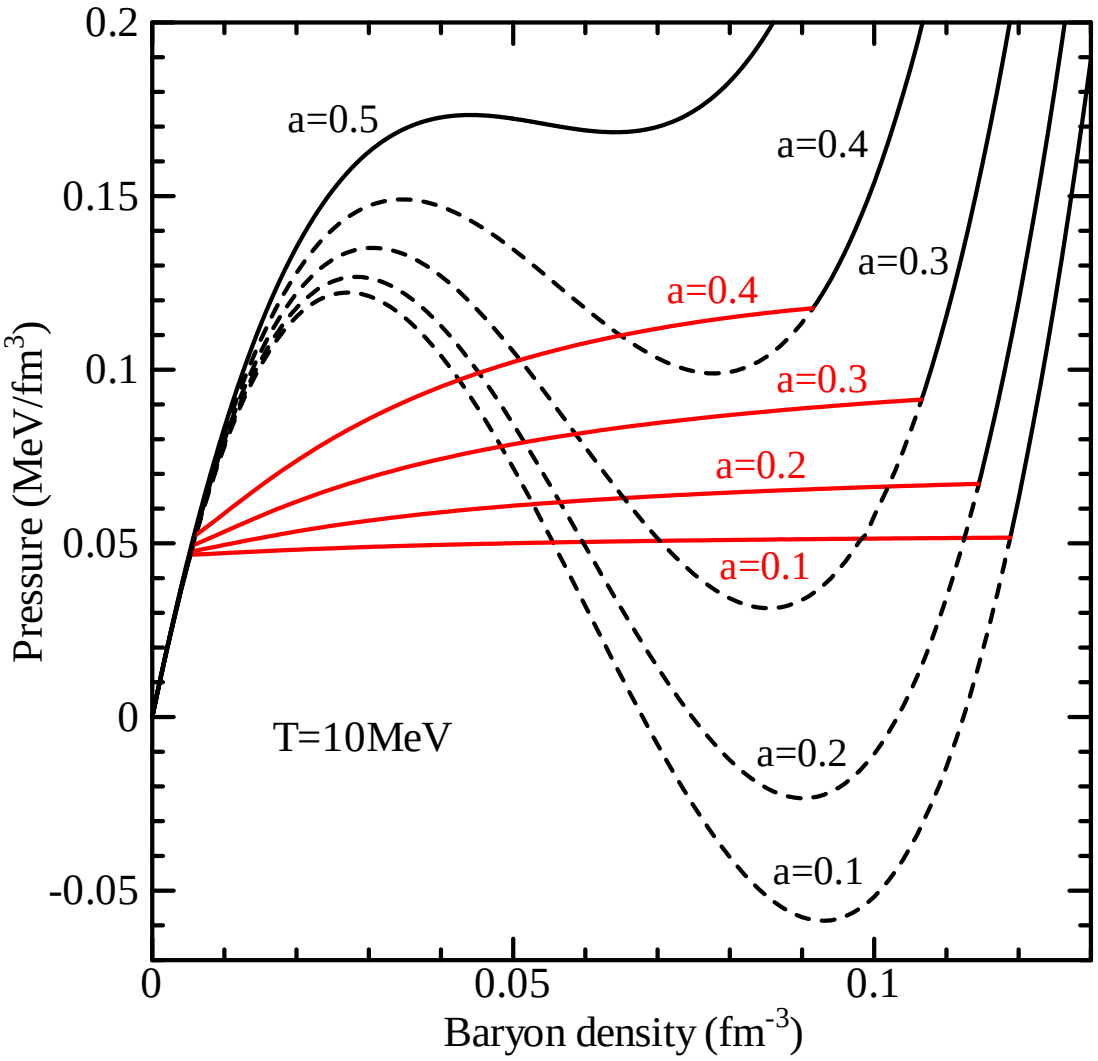

Figure 3: The pressure-density isotherms at $T = 10$MeV for the asymmetries from $a = 0.1$ to $a = 0.5$. The black dashed curves do not satisfy the Gibbs condition on phase equilibrium while the physically precise liquid-gas phase transitions are expressed by the red curves.

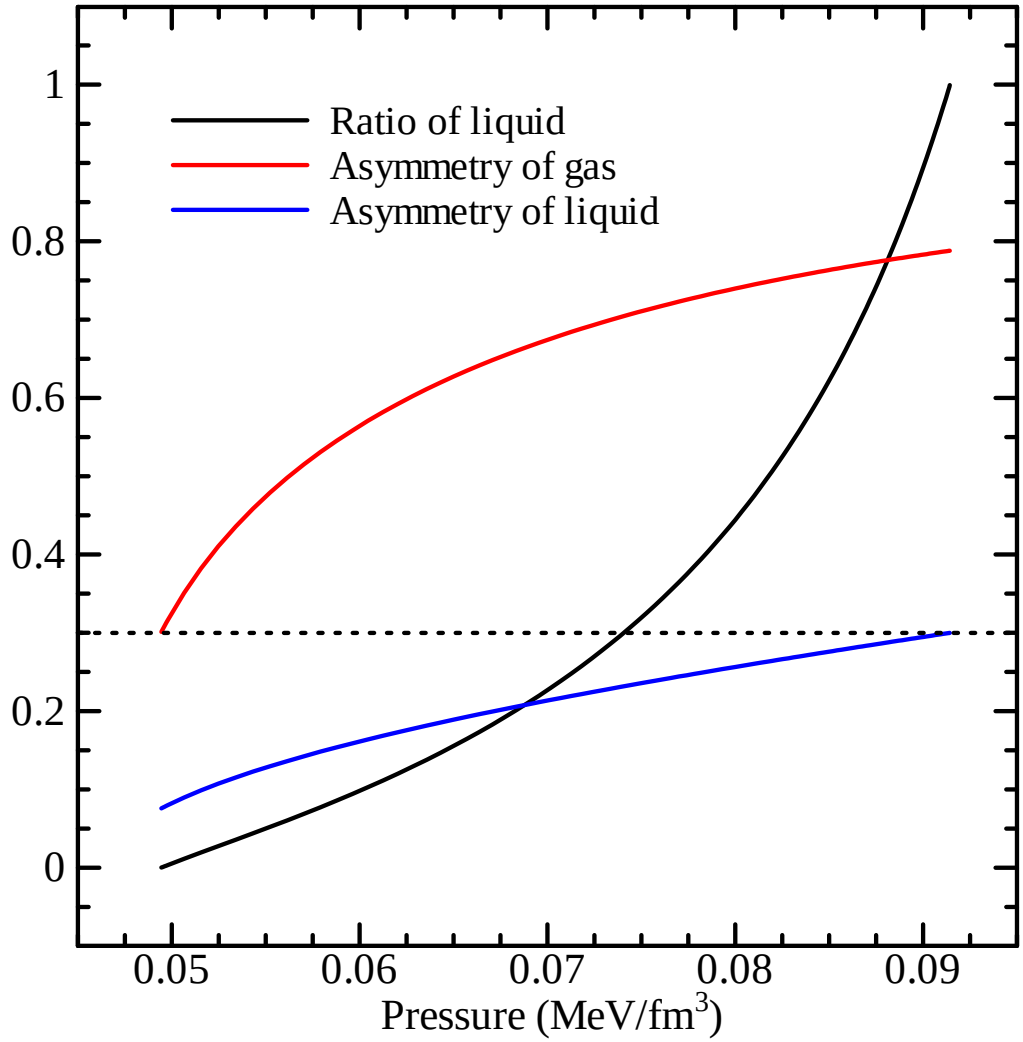

Figure 4: The black curve is the ratio of liquid $f_l = 1 - f_g$ in the liquid-gas phase transition for $T = 10$MeV and $a = 0.3$. The red and blue curves are the asymmetries in gaseous and liquid phases, $a_g = \frac{\left(\rho_{Bn}^{(g)} - \rho_{Bp}^{(g)}\right)}{\left(\rho_{Bn}^{(g)} + \rho_{Bp}^{(g)}\right)}$ and $a_l = \frac{\left(\rho_{Bn}^{(l)} - \rho_{Bp}^{(l)}\right)}{\left(\rho_{Bn}^{(l)} + \rho_{Bp}^{(l)}\right)}$.

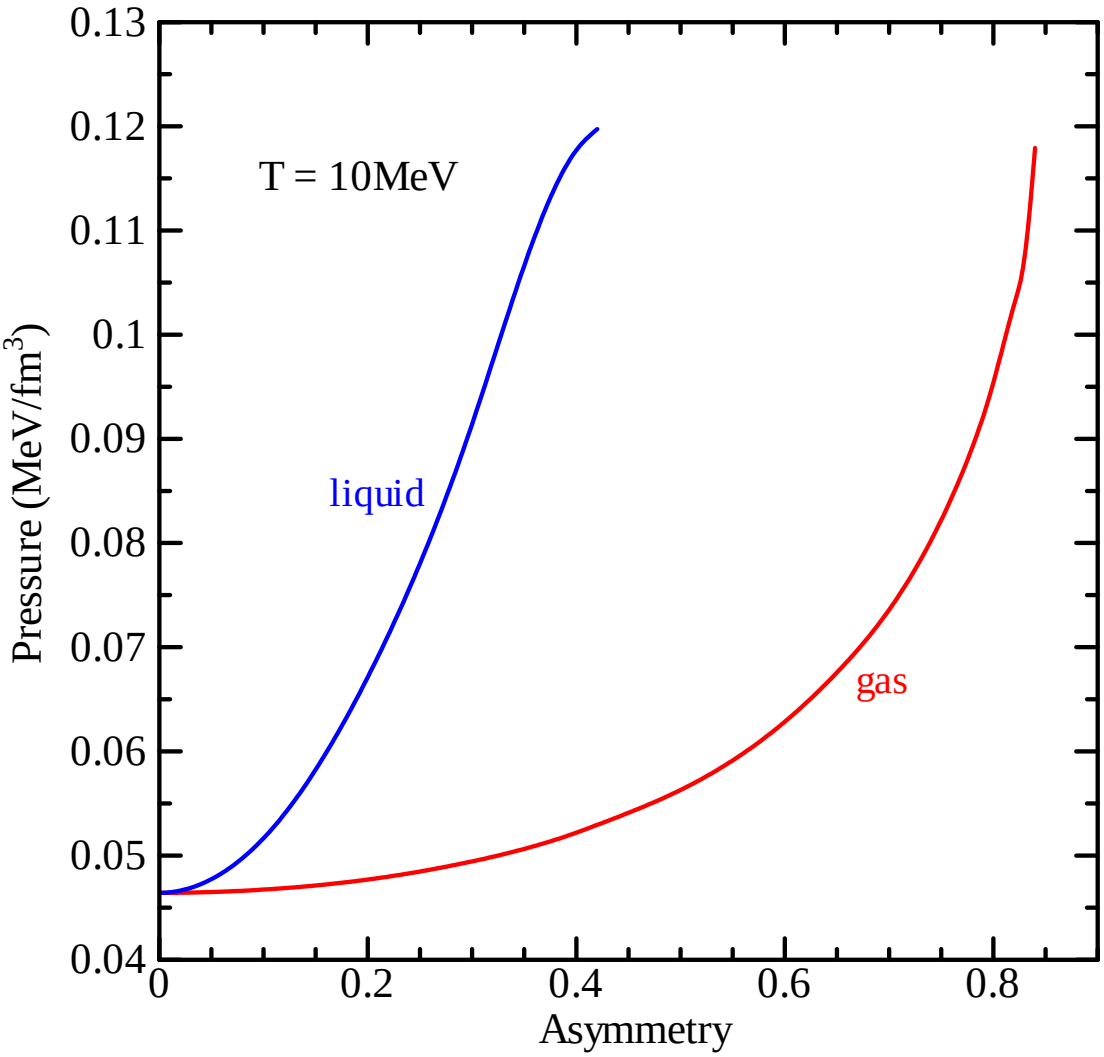

Figure 5: The section of binodal surface at $T = 10$MeV.

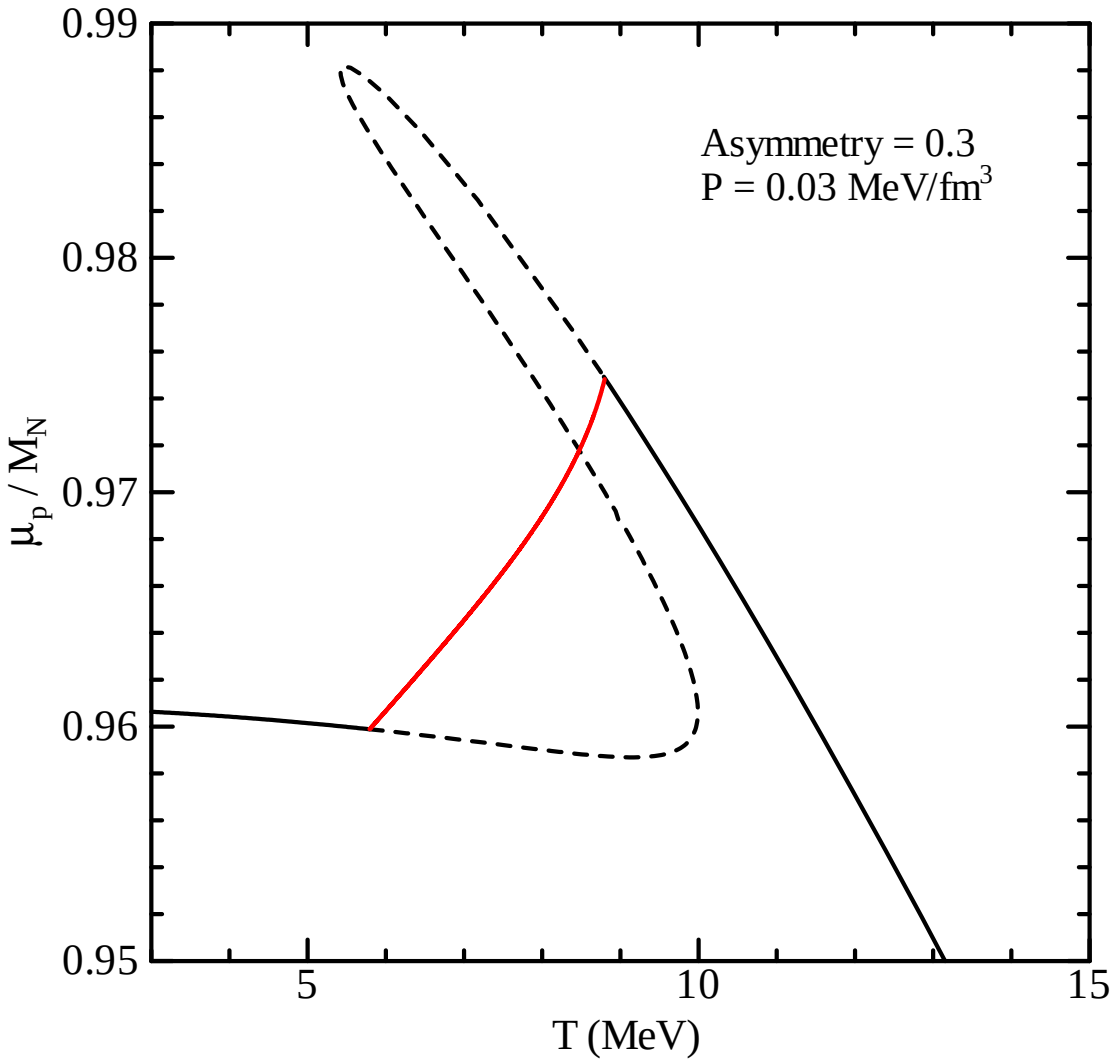

Figure 6: The proton chemical potential as a function of physical temperature for $P = 0.03\mathrm{MeV/fm}^3$ and $a = 0.3$. The black dashed curve does not satisfy the Gibbs condition on phase equilibrium while the physically precise liquid-gas phase transition is expressed by the red curve.

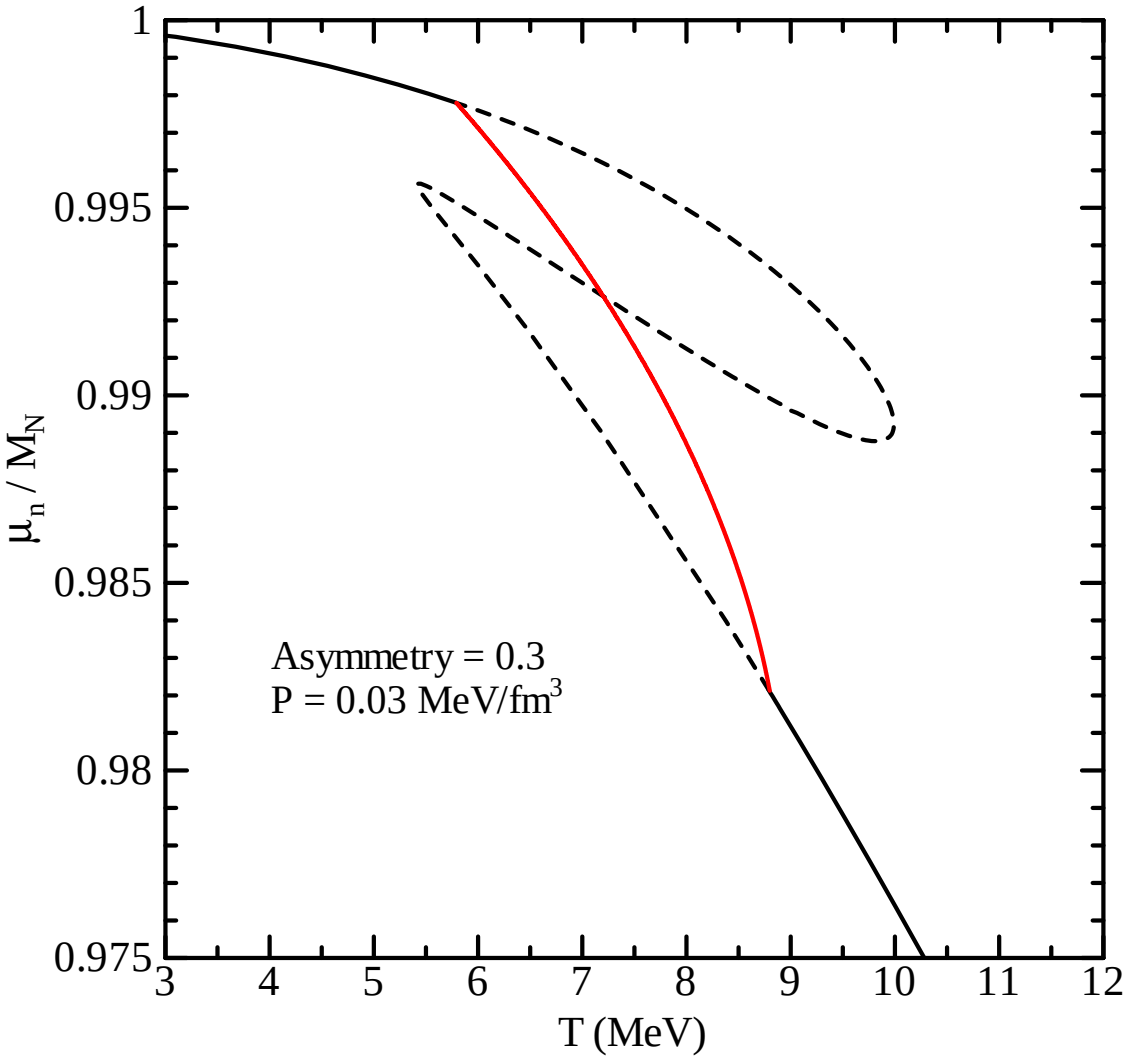

Figure 7: The same as Fig. 6 but for neutron chemical potential.

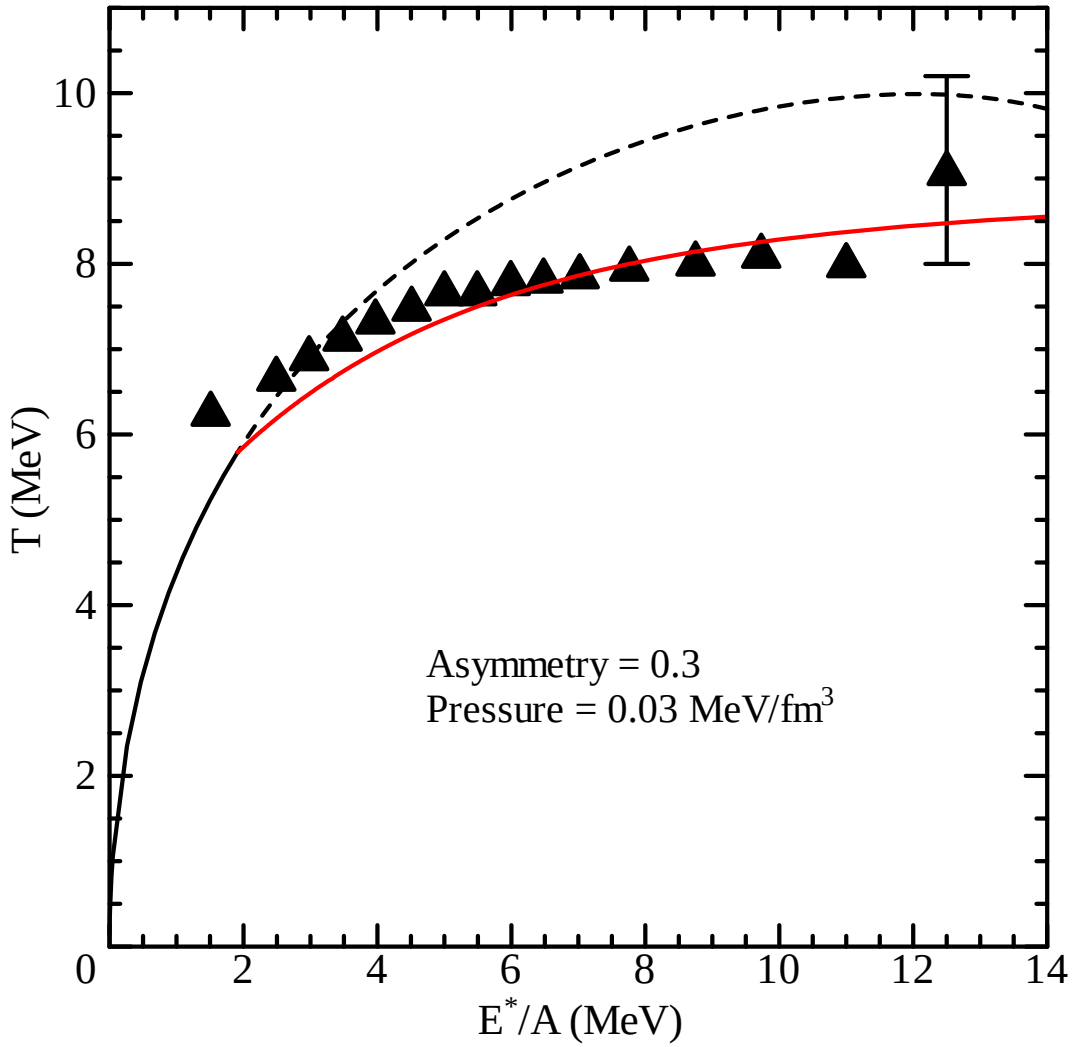

Figure 8: The caloric curves for $P = 0.03\mathrm{MeV/fm^3}$ and $a = 0.3$. The black solid curve represents the pure liquid phase. The black dashed curve does not satisfy the Gibbs condition on phase equilibrium while the physically precise liquid-gas mixed phase is expressed by the red curve.

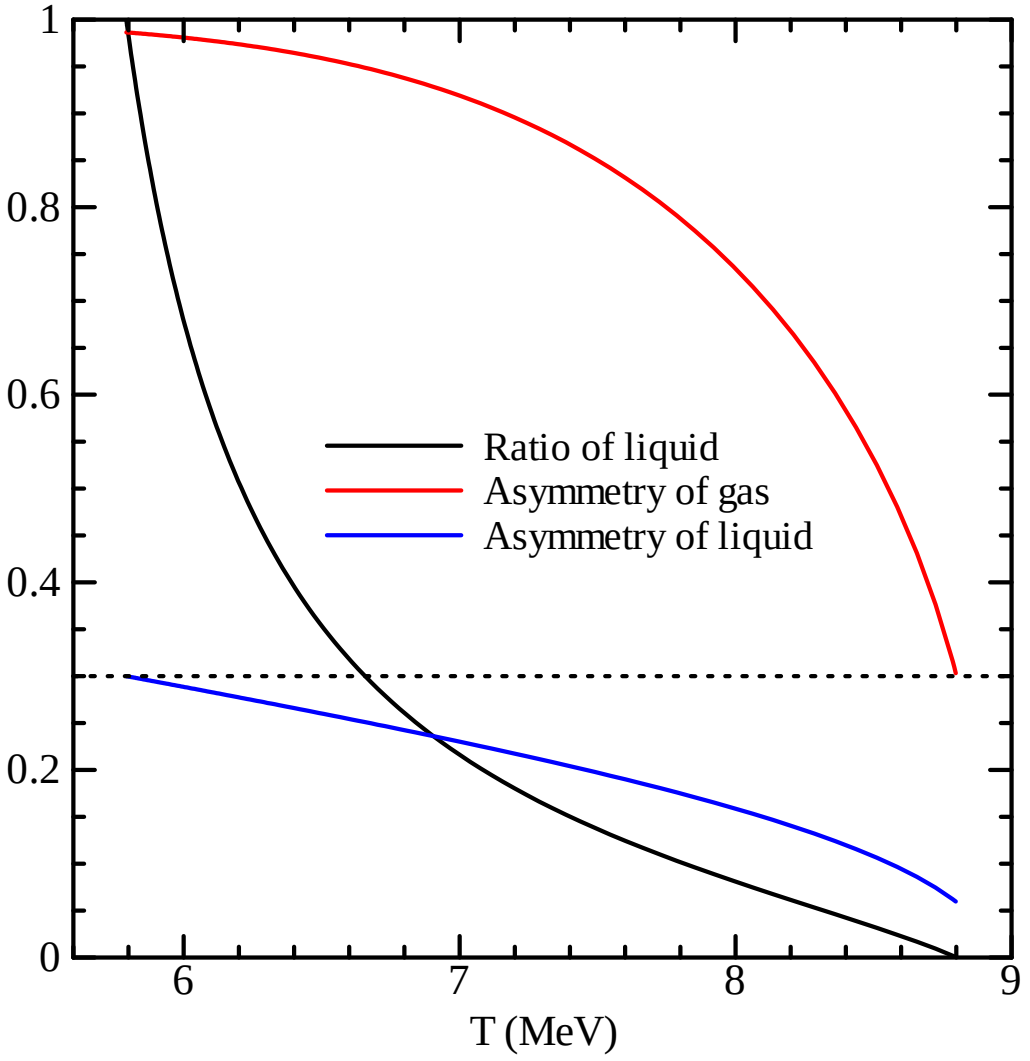

Figure 9: The black curve is the ratio of liquid $f_l = 1 - f_g$ in the liquid-gas phase transition for $P = 0.03\text{MeV/fm}^3$ and $a = 0.3$. The red and blue curves are the asymmetries in gaseous and liquid phases, $a_g = \frac{\left(\rho_{Bn}^{(g)} - \rho_{Bp}^{(g)}\right)}{\left(\rho_{Bn}^{(g)} + \rho_{Bp}^{(g)}\right)}$ and $a_l = \frac{\left(\rho_{Bn}^{(l)} - \rho_{Bp}^{(l)}\right)}{\left(\rho_{Bn}^{(l)} + \rho_{Bp}^{(l)}\right)}$.

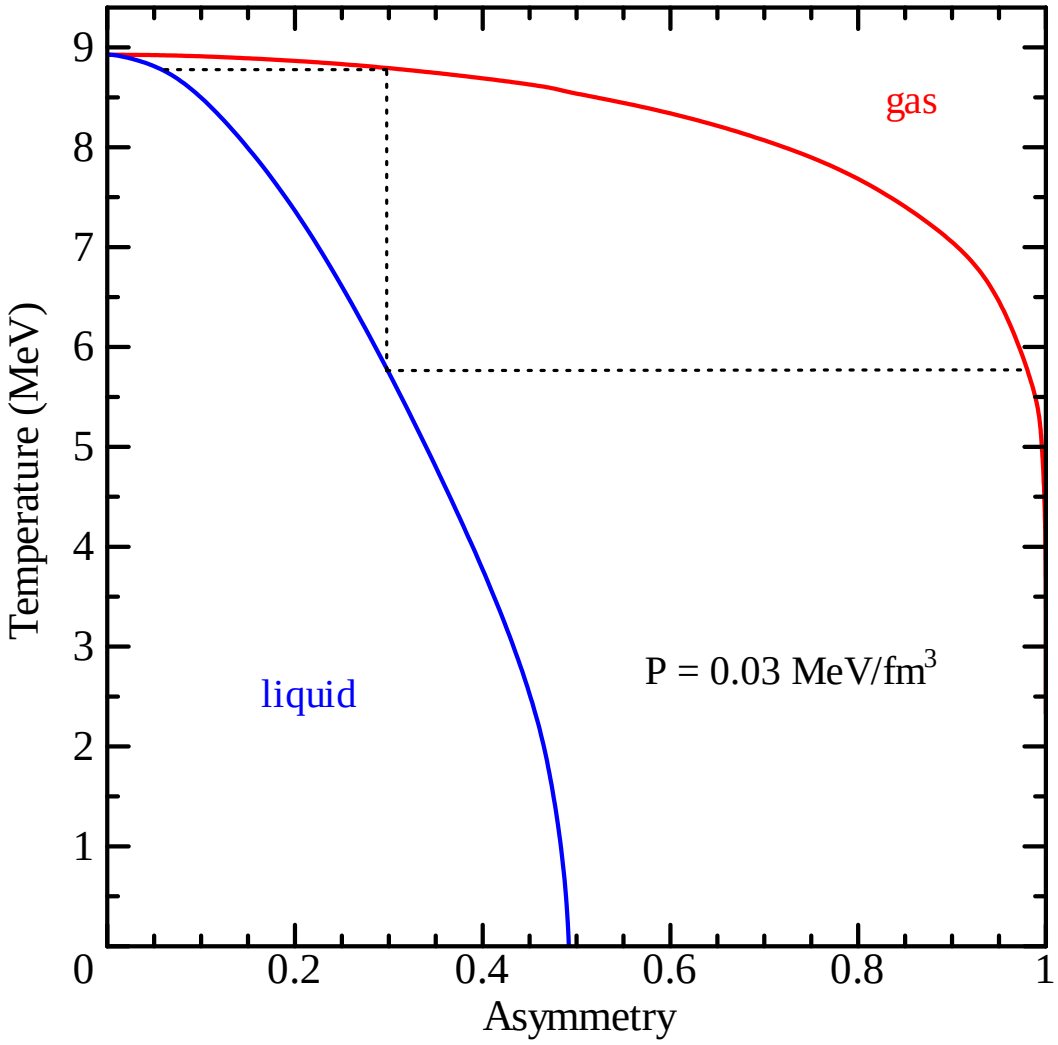

Figure 10: The boiling (red) and condensed (blue) curves of nuclear liquid and gas under constant pressure $P = 0.03\mathrm{MeV/fm}^3$.